

## Supplementary information

# Ultra-high performance flexible piezopotential gated In<sub>1-x</sub>Sn<sub>x</sub>Se phototransistor

*Christy Roshini Paul Inbaraj<sup>a,b,c</sup>, Roshan Jesus Mathew<sup>a, b,d</sup>, Golam Haider<sup>c</sup>, Tzu-Pei Chen<sup>b, c</sup>, Rajesh Kumar Ulaganathan<sup>e</sup>, Raman Sankar<sup>e,f</sup>, Krishna Prasad Bera<sup>b, c</sup>, Yu-Ming Liao<sup>b, c</sup>, Monika Kataria<sup>d,g,h</sup>, Hung-I Lin<sup>c</sup>, Fang Cheng Chou<sup>e</sup>, Yit-Tsong Chen<sup>d,i</sup>, Chih-Hao Lee<sup>a</sup>, and Yang-Fang Chen<sup>\*, c</sup>*

<sup>a</sup>Department of Engineering and System Science, National Tsing Hua University, Hsinchu 30013, Taiwan.

<sup>b</sup>Nano-Science and Technology Program, Taiwan International Graduate Program, Academia Sinica, Taipei 11529, Taiwan.

<sup>c</sup>Department of Physics, National Taiwan University, Taipei 10617, Taiwan.

<sup>d</sup>Institute of Atomic and Molecular Sciences, Academia Sinica, Taipei 10617, Taiwan.

<sup>e</sup>Center for Condensed Matter Sciences, National Taiwan University, Taipei 10617, Taiwan.

<sup>f</sup>Institute of Physics, Academia Sinica, Taipei 11529, Taiwan.

<sup>g</sup>Department of Physics, National Central University, Chung-Li 320, Taiwan.

<sup>h</sup>Molecular Science and Technology Program, Taiwan International Graduate Program, Academia Sinica, Taipei 11529, Taiwan.

<sup>i</sup>Department of Chemistry, National Taiwan University, Taipei, 10617, Taiwan.

## Corresponding Author

\*(Y.F.C.) E-mail: yfchen@phys.ntu.edu.tw

## Supplementary Note 1, Material characteristics

The elemental mapping for the bulk InSnSe crystal was carried out with field-emission scanning electron microscopy (FE-SEM) equipped with energy dispersive X-ray spectroscopy (EDAX) as shown below (**Figure S1**). The EDAX mappings of the In, Sn and Se elements supports their homogeneous distribution in the scanned area (**Figure S1a**) and the EDAX spectrum substantiates the presence of elements (**Figure S1b**).

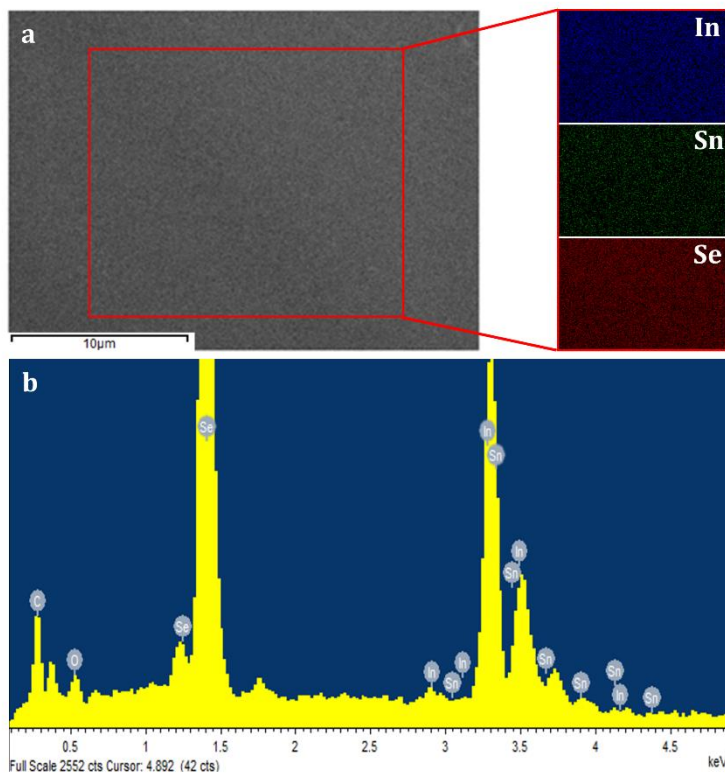


**Figure S1.** (a) FE-SEM image of the bulk InSnSe crystal with the elemental mapping for In, Sn and Se. (b) The EDAX spectrum of InSnSe crystal.

## Supplementary Note 2, Device characteristics

The few layered InSnSe flakes were exfoliated from InSnSe single crystals and transferred to the flexible substrate (Polyimide + PET) using polydimethylsiloxane (PDMS). Polyimide used here is commercially available Kapton® film (DuPont™). Atomic force microscopy (AFM) was used to identify the thickness of flakes. The electrodes (Cr/Au) were deposited after aligning the mask (from Cu grid for TEM) exactly on the sample using custom made micromanipulator. The photogain ( $\eta$ ) of the device with different laser power illumination ( $\lambda = 633$  nm) is illustrated in **Figure S2a**. The maximum photogain obtained is  $\eta = 1195$  with minimum laser power of  $7.021 \mu\text{W cm}^{-2}$ . The photo-switching characteristics of the photodetector obtained with the laser illumination ( $P = 132.5 \mu\text{W cm}^{-2}$ ) at  $V_{ds} = 1$  V is shown in **Figure S2b**. The response time and recovery time of the device is 0.23 s and 0.24 s, respectively (**Figure S2c, d**). Though the previous works on transition metal dichalcogenides based photodetectors reports response time in the range of millisecond and microsecond,<sup>1–3</sup> we measured the response time of InSnSe photodetector to be 0.23 s which is due to the limitation in our measurement setup. In order to figure out the enhancement or effect of InSnSe layer, the current generated on laser illumination ( $I_{light}$ ) has been normalized with  $I_0$  value of InSnSe device without the application of strain as shown in **Figure S3**. The enhancement of current in the InSnSe device on laser illumination ( $P = 132.48 \mu\text{W cm}^{-2}$ ) with applied bias ( $V_{ds} = 1$  V) is almost twice due to InSnSe layer.

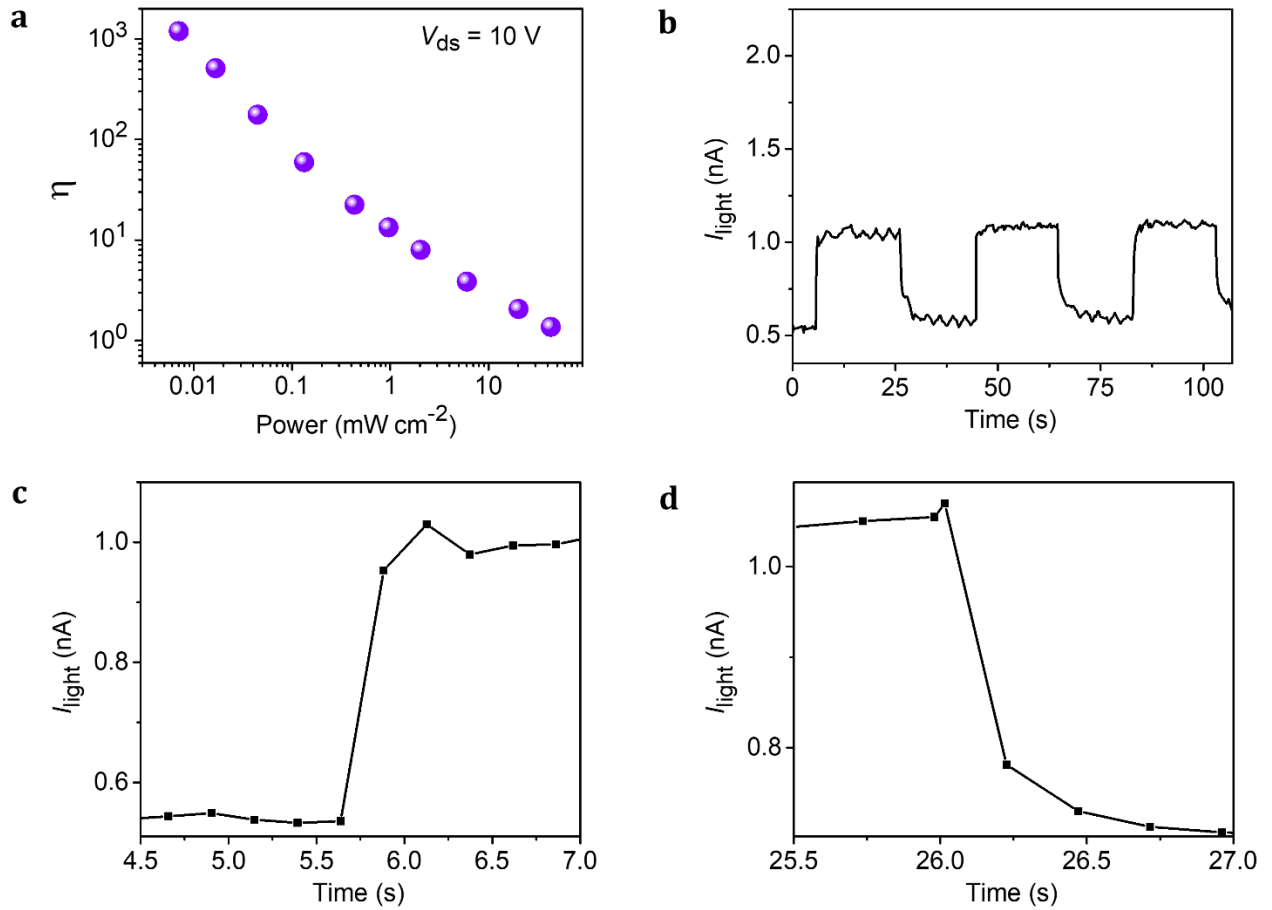


**Figure S2.** (a) Photogain at  $V_{ds} = 10 \text{ V}$  as a function of different laser power intensity measured in the planar state. (b) The photo-switching characteristics of the device in the plane state at  $V_{ds} = 1 \text{ V}$  with the illuminated laser power as  $P = 132.48 \mu\text{W cm}^{-2}$ . (c) and (d) are the representation of device response on laser illumination and de-excitation on removal of laser illumination, respectively.

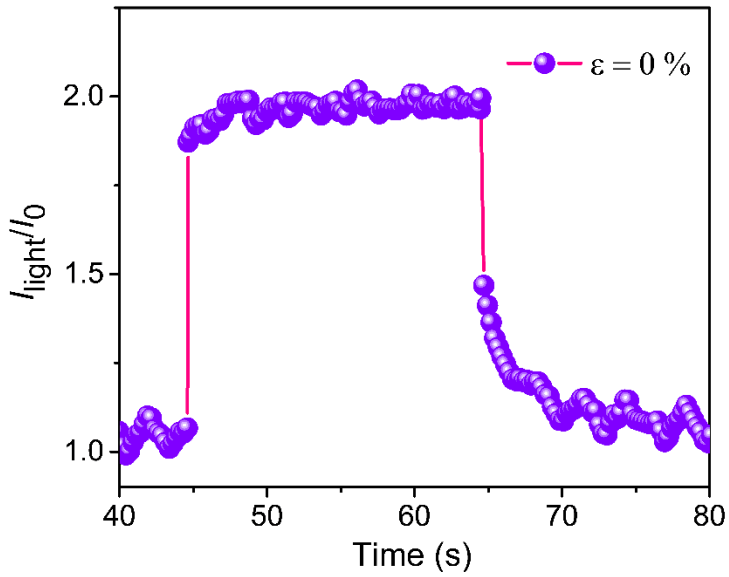


**Figure S3.**  $I_{\text{light}} / I_0$  verus time at  $V_{\text{ds}} = 1$  V and  $P = 132.48 \mu\text{W cm}^{-2}$  without strain showing the enhancement of current due to InSnSe layer.

### Supplementary Note 3, Mechanical strain

In order to induce mechanical strain in the device, it is bent with different radius of curvature. The applied strain is calculated using the formula  $\varepsilon = (t/2R_c) \times 100 \%$ , where  $t$  is the thickness of the substrate and  $R_c$  is the radius of curvature (**Figure S4a**). To obtain different radius of curvature, the device on polyimide/PET substrate is bent over rigid rods of different diameters as shown in **figure S4b**.

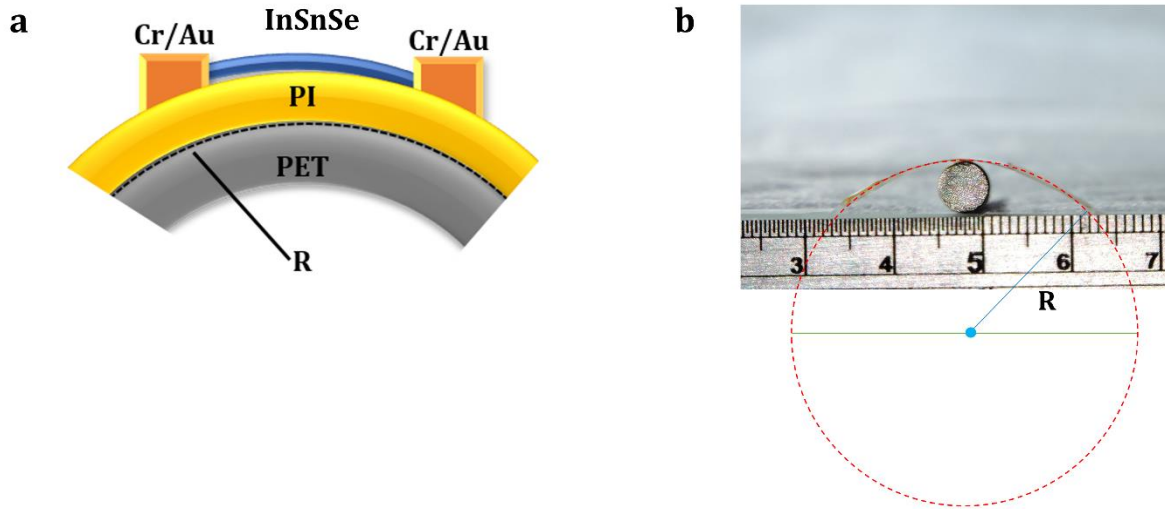


**Figure S4.** Flexible device. (a) Schematic representation of the bent state to induce strain in the device. (b) Photograph representing the real device under bending condition.

#### Supplementary Note 4, Device characteristics under strain

The electrical transport measurement was carried out for the device in the strained condition. The drain-source current increases along the applied bias under laser illumination. When the mechanical strain is induced, the drain-source current further increases for the applied bias at the same laser power. The  $I_{ds}$ - $V_{ds}$  plots for the InSnSe device at different strain conditions under the laser illumination power of  $132.48 \mu\text{W cm}^{-2}$  and  $7.021 \mu\text{W cm}^{-2}$  are represented in **Figure S5a** and **S5b**, respectively. The generated photocurrent for the applied voltage bias at different mechanical strain and constant laser power is depicted in **Figure S6**. The inset of **Figure S6a** shows the photocurrent observed at zero drain bias. This is because of the piezoelectric potential generated while bending the device which manifests its use in fabricating self-powered devices. The maximum photocurrent observed at a laser power of  $2.03 \text{ mW cm}^{-2}$  increases from  $\sim 15 \text{ nA}$  to  $\sim 60 \text{ nA}$  under the mechanical strain of  $2.7\%$  (**Figure S6d**). Hence, the photoresponsivity of the device increases under applied strain. The photoresponsivity (R) and detectivity ( $D^*$ ) of the

device as a function of illuminated laser power and at different strain conditions is depicted in **Figure S7**. Similarly, the photogain of the device at different strains is shown in **Figure S8**.

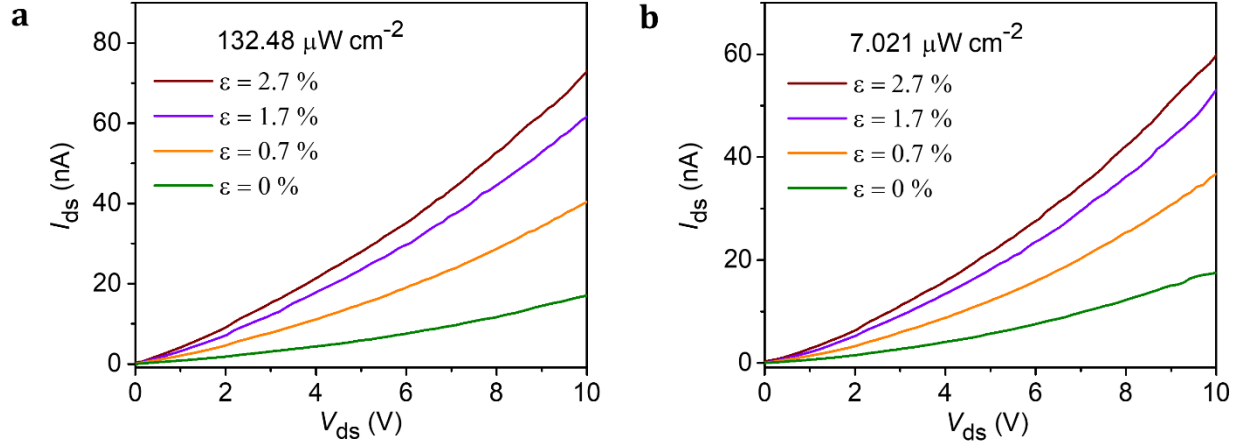


**Figure S5.** Device characteristics in the bent state. The  $I_{ds} - V_{ds}$  characteristic curves measured at different strains at illuminated laser power (a)  $132.48 \mu\text{W cm}^{-2}$  and (b)  $7.021 \mu\text{W cm}^{-2}$ , respectively.

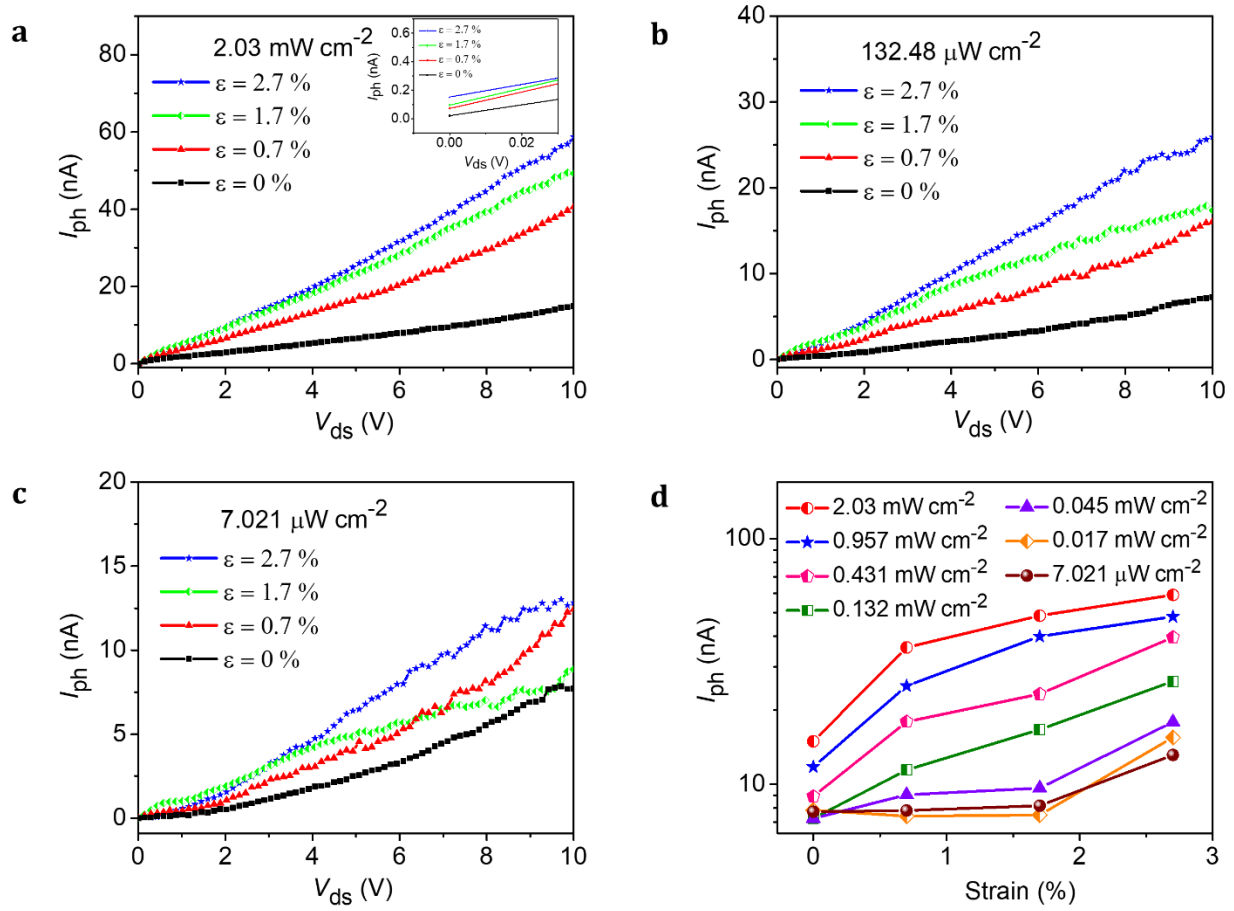
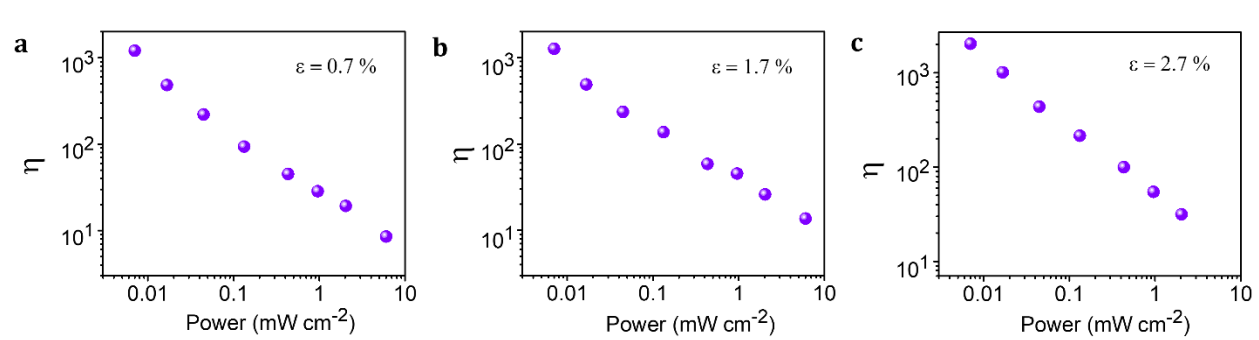
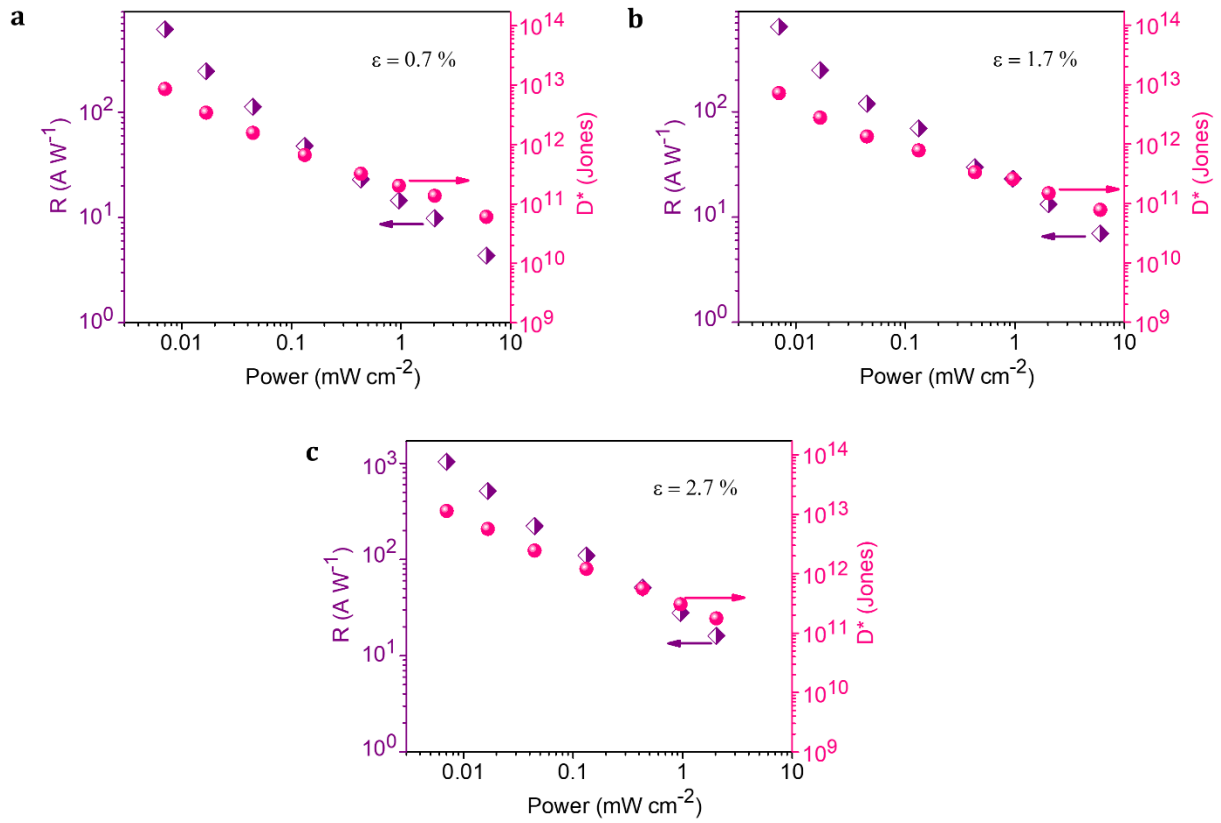


**Figure S6.** Piezo-phototronic effect. The generated photocurrents as a function of  $V_{\text{ds}}$  at different strains and illuminated laser power intensities of (a)  $2.03 \text{ mW cm}^{-2}$ , (b)  $132.48 \mu\text{W cm}^{-2}$  and (c)  $7.021 \mu\text{W cm}^{-2}$ , respectively. (d) Photocurrent as a function of strain at different laser power illuminations.



## Supplementary Note 5, Raman spectrum

The Raman spectrum was measured for InSnSe device at different strain condition. **Figure S9a** shows the deconvoluted peaks of  $A^{1g}$  mode at different strains and the extended figure clearly depicts the peaks at  $102\text{ cm}^{-1}$ ,  $110\text{ cm}^{-1}$  and  $120\text{ cm}^{-1}$ . The deconvolution of  $A^{2g}$  mode at different strain is represented in **Figure S9b** and the peaks at  $215\text{ cm}^{-1}$ ,  $222\text{ cm}^{-1}$ ,  $229\text{ cm}^{-1}$  and  $235\text{ cm}^{-1}$  are made clear in the extended figure.

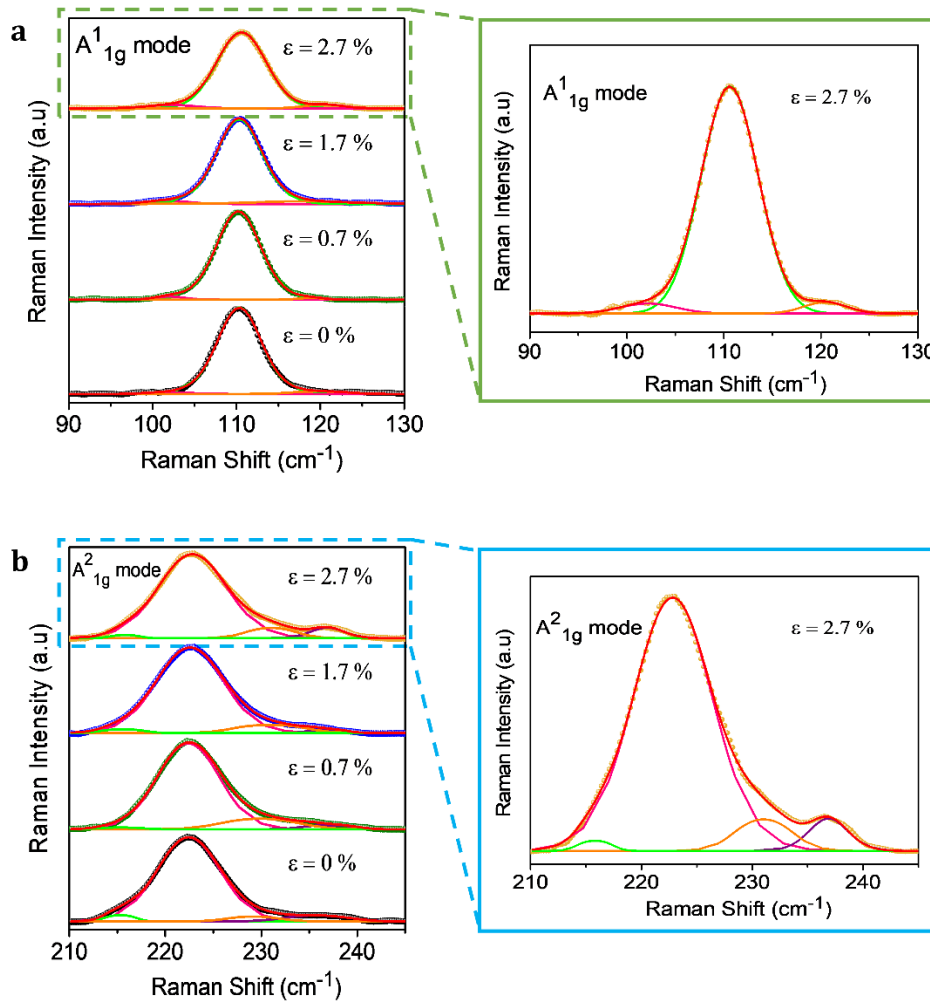


**Figure S9.** Raman spectrum. (a) and (b), deconvoluted peaks of  $A^{1g}$  and  $A^{2g}$  phonon mode, respectively.

## Supplementary Note 6, Internal strain

The minor blue shift observed in the deconvoluted peak of  $E^2_{1g}$  phonon mode in the Raman spectrum under strain is shown in **Figure S10**. The internal strain acting in In-Se bond based on the Raman shift was calculated as follows.

The effective mass (m) of In and Se in  $In_{0.9}Sn_{0.1}Se$  is given by,

$$m = \frac{0.9M_{In} \times M_{Se}}{0.9M_{In} + M_{Se}} \quad (1)$$

where  $M_{In}$  and  $M_{Se}$  are the atomic mass of indium and selenium, respectively.

The force constant k (in unit of  $N\text{ cm}^{-1}$ ) is estimated from the relation,

$$\nu = \frac{1}{2\pi c} \sqrt{\frac{k}{m}} \quad (2)$$

where  $\nu$  is the Raman wavenumber,  $c$  is the speed of light and  $m$  is the effective mass.

The bond length (L) (in unit of  $\text{\AA}$ ) is deduced from the formula<sup>4</sup>,

$$k = \frac{1.86 \times 10^5}{(L-d)^3} \quad (3)$$

Where the constant d is calculated for the equilibrium bond length of In-Se ( $2.54\text{ \AA}$ )<sup>5</sup> and internal strain in the In-Se bond is calculated with the change in bond length as,

$$\varepsilon_{int} = \frac{\Delta L}{L} \times 100 \% \quad (4)$$

where  $\Delta L$  is the change in bond length and L is the bond length at 0% strain.

The calculated values of force constant, bond length and the resultant internal strain are tabulated as in **Table S1**.

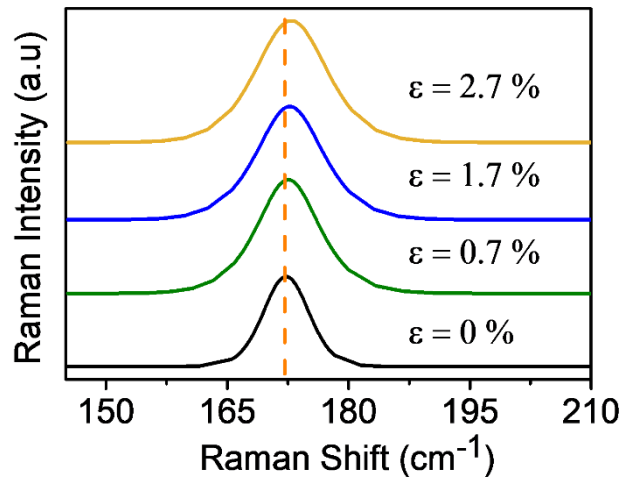


**Figure S10.** The representation of Raman shift in deconvoluted peak of  $E^2_{1g}$  phonon mode.

**Table S1.** The calculated force constant, bond length and internal strain corresponding to the Raman shift of  $E^2_{1g}$  mode.

Mechanical Strain (%)	Raman wavenumber ( $\text{cm}^{-1}$ )	Force constant ( $\text{N cm}^{-1}$ )	Bond length ( $\text{\AA}$ )	Internal strain (%)
0	172.275	0.77738	2.540	0
0.7	172.541	0.77978	2.538	0.054
1.7	172.732	0.78151	2.537	0.093
2.7	172.914	0.78316	2.536	0.130

### Supplementary Note 7, Wearable device

The wearable property of the photodetector was demonstrated by measuring the electrical transport property of the device by adhering the polyimide tape to a pen and a nitrile glove, as shown in **Figure S11**.

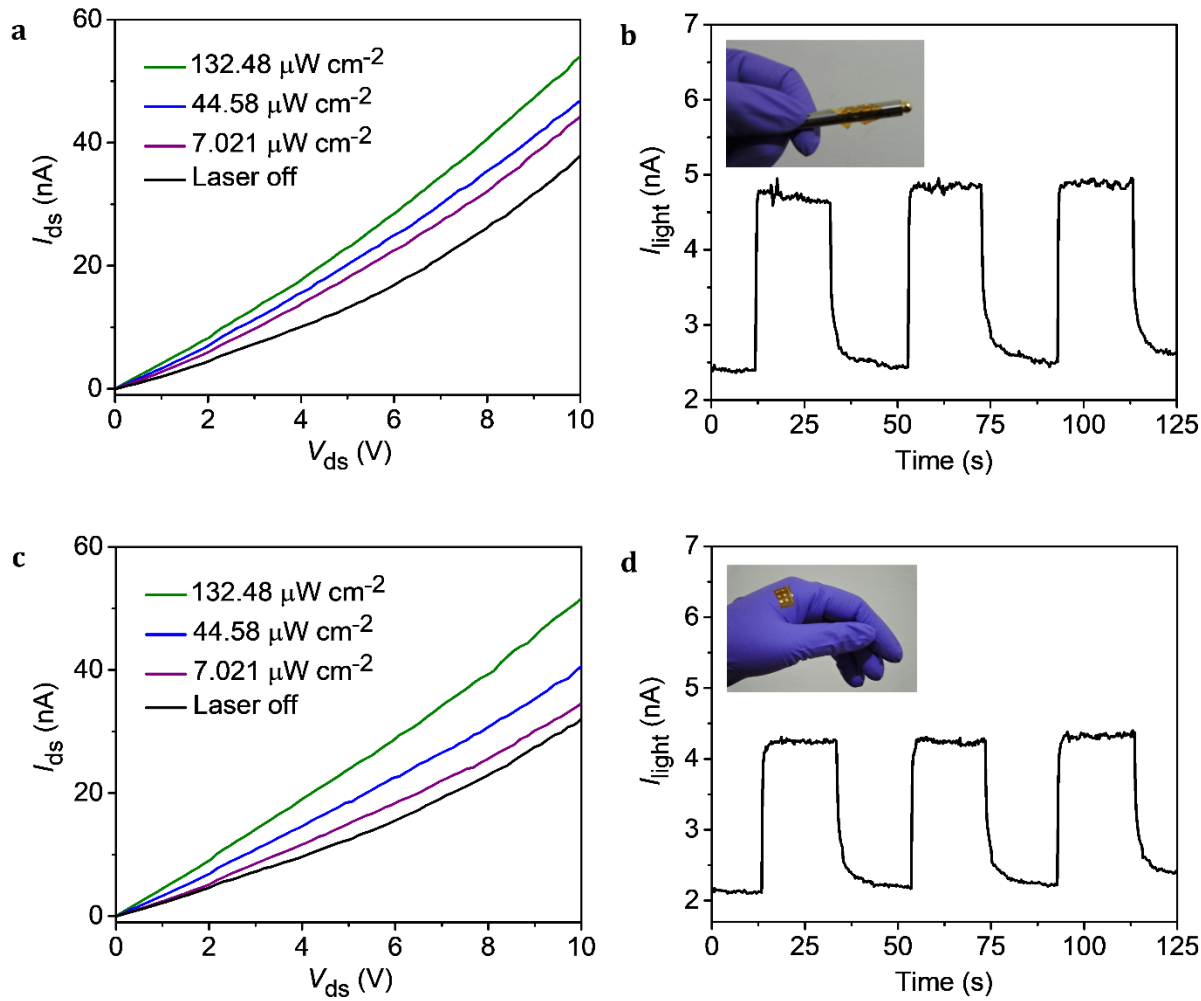


**Figure S11.** Wearable Photodetector. (a) and (c) are the  $I_{ds}$ - $V_{ds}$  characteristic curves measured at different laser power intensities when the device is attached over a pen and glove, respectively. (b) and (d) are the photo-switching characteristics of the device while attached on a pen and glove, respectively.

### **Supplementary Note 8, Piezophototronic effect**

In the reported InSnSe phototransistor, the application of gate voltage is replaced by the piezopotential generated due to piezoelectric effect in the material under strain. The piezoelectric effect of InSnSe in phototransistor in additional devices as shown in **Figure S12** in order to substantiate the repeatability of our material performance. Under the application of strain in the dark condition, the drain-source current increases due to the piezopotential generated in the material while bending. When the laser is illuminated on the device, this piezopotential acts as an additional bias in enhancing the photocurrent generation replacing the gate voltage. This makes InSnSe as a potential candidate for the fabrication of two-terminal piezopotential gated phototransistors. The variation of responsivity with the application of strain ( $R_e = 2.7\% / R_e = 0\%$ ) for five devices are shown in **Figure S13**. The average enhancement of the responsivity with 2.7% tensile strain for the fabricated phototransistor is  $2.2 \pm 0.7$  times.

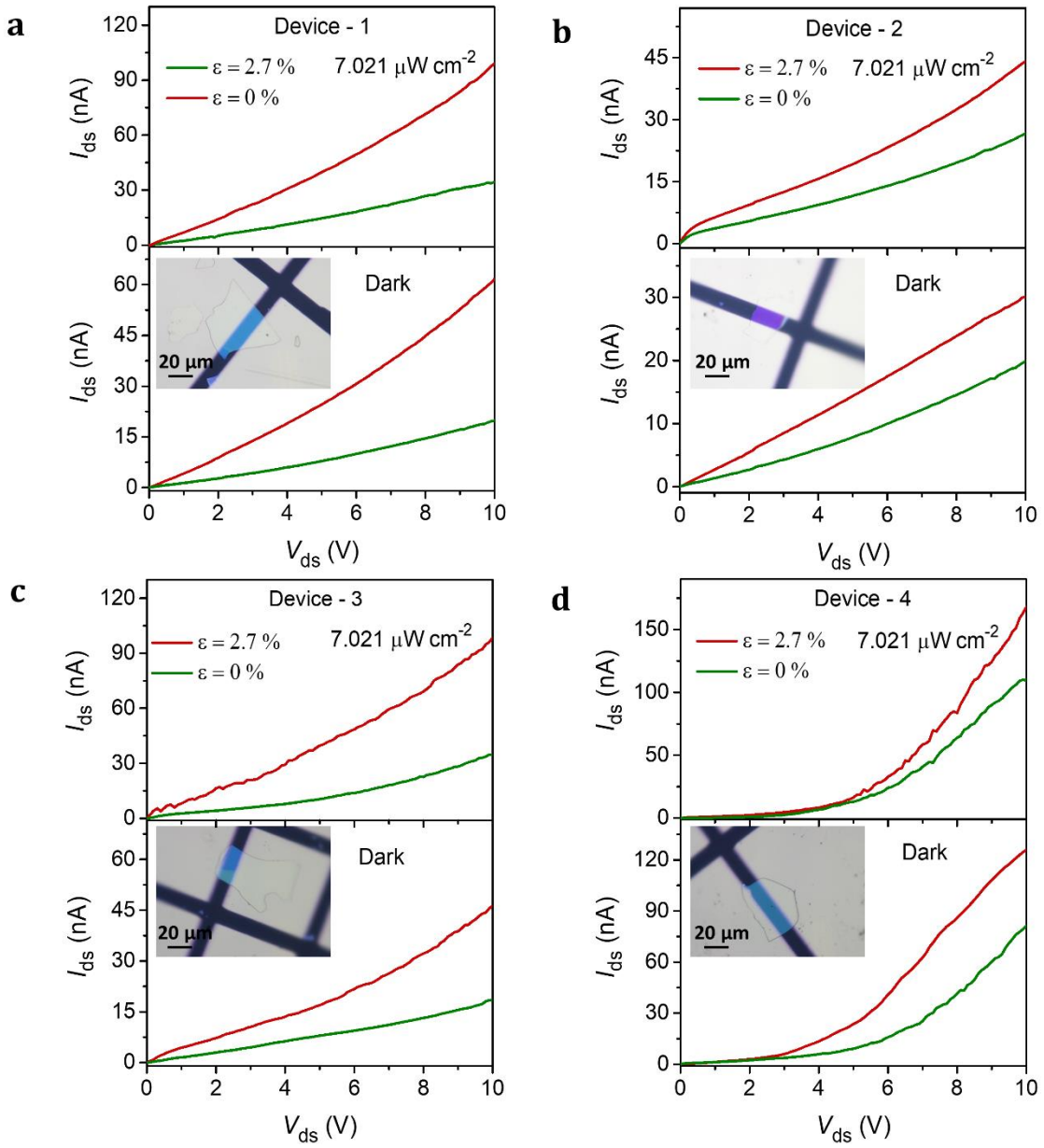


**Figure S12.** Piezophototronic effect. (a), (b), (c) and (d) The  $I_{ds}$ - $V_{ds}$  characteristic curves in the dark and laser illuminated condition under the application of devices. The inset depicts the optical microscopy image of the measured devices.

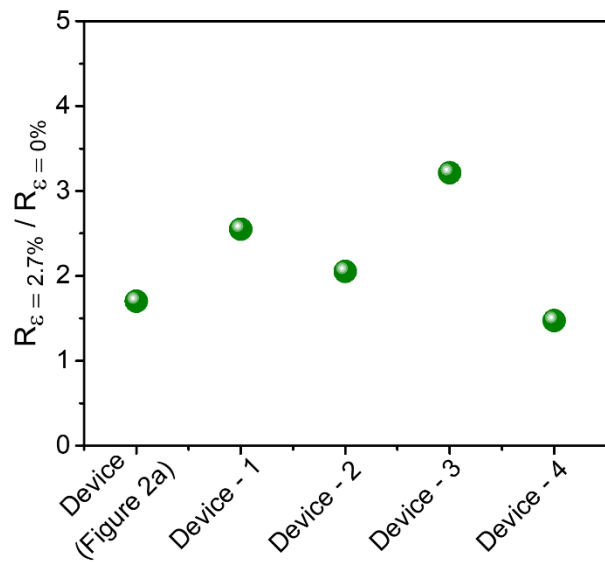


**Figure S13.** Variation in the performance of InSnSe devices.

## Reference

- (1) Su, G.; Hadjiev, V. G.; Loya, P. E.; Zhang, J.; Lei, S.; Maharjan, S.; Dong, P.; M. Ajayan, P.; Lou, J.; Peng, H. Chemical Vapor Deposition of Thin Crystals of Layered Semiconductor SnS<sub>2</sub> for Fast Photodetection Application. *Nano Lett.* **2015**, *15* (1), 506–513.
- (2) Lei, S.; Ge, L.; Najmaei, S.; George, A.; Kappera, R.; Lou, J.; Chhowalla, M.; Yamaguchi, H.; Gupta, G.; Vajtai, R.; Mohite, A. D.; Ajayan, P. M. Evolution of the Electronic Band Structure and Efficient Photo-Detection in Atomic Layers of InSe. *2014*, *8* (2), 1263–1272.
- (3) Tamalampudi, S. R.; Lu, Y. Y.; Kumar U., R.; Sankar, R.; Liao, C. Da; Moorthy B., K.; Cheng, C. H.; Chou, F. C.; Chen, Y. T. High Performance and Bendable Few-Layered InSe Photodetectors with Broad Spectral Response. *Nano Lett.* **2014**, *14* (5), 2800–2806.
- (4) Badger, R. M. A Relation between Internuclear Distances and Bond Force Constants. *J.Chem.Phys.* **1934**, *2*, 128–131.
- (5) Xue, C.; Hu, D.; Zhang, Y.; Yang, H.; Wang, X.; Wang, W.; Wu, T. Two Unique Crystalline Semiconductor Zeolite Analogues Based on Indium Selenide Clusters. *Inorg.Chem.* **2017**, *56* (24), 14763–14766.